© 2022. Published by The Company of Biologists Ltd | Development (2022) 149, dev200569. doi:10.1242/dev.200569

RESEARCH ARTICLE

Chondroitin sulfate enhances the barrier function of basement membrane assembled by heparan sulfate

Chenqi Tao[1,‡], Neoklis Makrides[1], Jen-Zen Chuang[2], Yihua Wu[1], Steven E. Brooks[*,1], Jeffrey D. Esko[3], Ching-Hwa Sung[2] and Xin Zhang[1,4,‡]

ABSTRACT

Glycosaminoglycans are ubiquitously expressed polysaccharides that are attached to proteoglycans. Here, we showed that ablation of the heparan sulfate (HS) polymerase Ext1 in retinal progenitor cells did not affect initial progression of retinal angiogenesis, but it disrupted the pruning of blood vessels and establishment of arterioles and venules. In the absence of retinal HS, blood vessels were also vulnerable to high oxygen tension in early postnatal stages, which could be rescued by exogenous vascular endothelial growth factor (VEGF), consistent with the role of retinal HS in the fine-tuning of VEGF signaling. Furthermore, we observed that the retinal inner limiting membrane (ILM) was disrupted by deletion of *Ext1* in a timing-specific manner, suggesting that retinal HS is required for the assembly but not the maintenance of the basement membrane. Lastly, we showed that further deletion of C4st1, a chondroitin sulfate (CS) sulfation enzyme, did not affect the assembly of the ILM but, when combined with *Ext1* deletion, it aggravated the retinal permeability by disrupting the retinal glycocalyx. These results demonstrate an important role of CS and HS in establishing the barrier function of the extracellular matrix.

KEY WORDS: Retina, Chondroitin sulfate, Astrocyte, Basement membrane, Angiogenesis, Glycocalyx

INTRODUCTION

Glycosaminoglycans (GAGs) are a family of ubiquitously expressed polysaccharides that play important roles in development and physiology (Bishop et al., 2007; Mikami and Kitagawa, 2013; Mizumoto et al., 2013). Based on their composition, these macromolecules are classified into heparan sulfate (HS), chondroitin sulfate (CS), dermatan sulfate (DS) and keratan sulfate (KS). GAG synthesis requires cascades of enzymes, including enzymes involved in the generation of nucleotide sugar precursors and enzymes, such as Chsy/Chpf and Ext1/2 that assemble the backbone of CS/DS and HS chains, respectively (Fig. 1A; Mikami and Kitagawa, 2013; Mizumoto et al., 2013). During assembly of these chains, GAGs undergo various epimerization and sulfation reactions. In CS/DS, the sulfation reactions are catalyzed by members of the Chst family of enzymes, which add sulfate groups to the C4 and/or C6 positions of N-acetylgalactosamine residues and to iduronic acid residues in DS. In HS, Ndst isozymes catalyze the initial N-deacetylation and N-sulfation of the N-acetylglucosamine residues, which is then followed by the addition of sulfate groups to the C6 and C3 positions of glucosamine residues and to the C2 of uronic acids. The extent of these modifications varies, creating enormous structural complexity, which in turn tunes the selectivity of protein binding and subsequent biological activity.

Retinal angiogenesis is a prime example that illuminates the diverse functions of GAGs in development. In mice, formation of the retinal vasculature requires sequential migration of astrocytes and endothelial cells into the neonatal retina; both processes are dependent on retinal GAGs (Tao and Zhang, 2014). We have previously examined the impact of altering the enzyme Ugdh, which is responsible for the formation of UDP-glucuronic acid required for the assembly of CS/DS, HS and hyaluronan. Inactivation of Ugdh disrupted the inner limiting membrane (ILM) of the retina, which serves as the substratum for astrocyte migration (Tao and Zhang, 2016). HS has also been shown to interact with vascular endothelial growth factor (Vegf) produced by astrocytes, generating localized Vegf concentration gradients to attract the migration of endothelial cells into the retina (Ruhrberg et al., 2002; Stalmans et al., 2002). Mutation of the HS interaction motif in Vegfa leads to severe defects in vascular outgrowth and patterning. Therefore, migration of retinal astrocytes and endothelial cells requires the distinct functions of GAGs in basement membrane and VEGF signaling.

In this study, we further explored the roles of GAGs in retinal angiogenesis and astrocyte migration by genetically disrupting the biosynthesis of HS and CS. Surprisingly, unlike the profound angiogenesis defect observed in *Vegfa* mutants lacking HS interactions, deletion of the HS polymerase *Ext1* in the retina failed to perturb the initial expansion of the vasculature. Instead, loss of retinal HS impaired only vessel remodeling and maturation. On the other hand, the ILM was disrupted by deletion of *Ext1* in a time-dependent manner, suggesting that HS is required for the initial assembly but not for the maturation of the ILM. Lastly, we show that loss of the CS sulfation enzyme C4st1 (*Chst11*) did not cause an obvious retinal phenotype, but it synergized with *Ext1* deletion in breaching the barrier function of the ILM and retinal glycocalyx. These results reveal the distinct requirements of HS and CS in the assembly and function of the retinal extracellular matrix (ECM).

RESULTS

Retinal angiogenesis requires HS for remodeling but not outgrowth of the vasculature

Despite the widely accepted role of HS in VEGF signaling, the function of retinal HS in angiogenesis has not been directly tested. To this end, we abolished HS synthesis by ablating the HS

[1]Department of Ophthalmology, Columbia University, New York, NY 10032, USA. [2]Department of Ophthalmology, Dyson Vision Research Institute, Weill Cornell Medicine, New York, NY 10065, USA. [3]Department of Cellular and Molecular Medicine, Glycobiology Research and Training Center, University of California San Diego, La Jolla, CA 92093, USA. [4]Department of Pathology and Cell Biology, Columbia University, New York, NY 10032, USA.
*Present address: Department of Ophthalmology, Medical College of Georgia, Augusta, GA 30912, USA.

‡Authors for correspondence (ct2612@cumc.columbia.edu, xz2369@columbia.edu)

C.T., 0000-0002-4346-7343; J.D.E., 0000-0001-8322-1834; X.Z., 0000-0001-5555-0825

Handling Editor: Liz Robertson
Received 25 January 2022; Accepted 5 May 2022

Development (2022) 149, dev200569. doi:10.1242/dev.200569

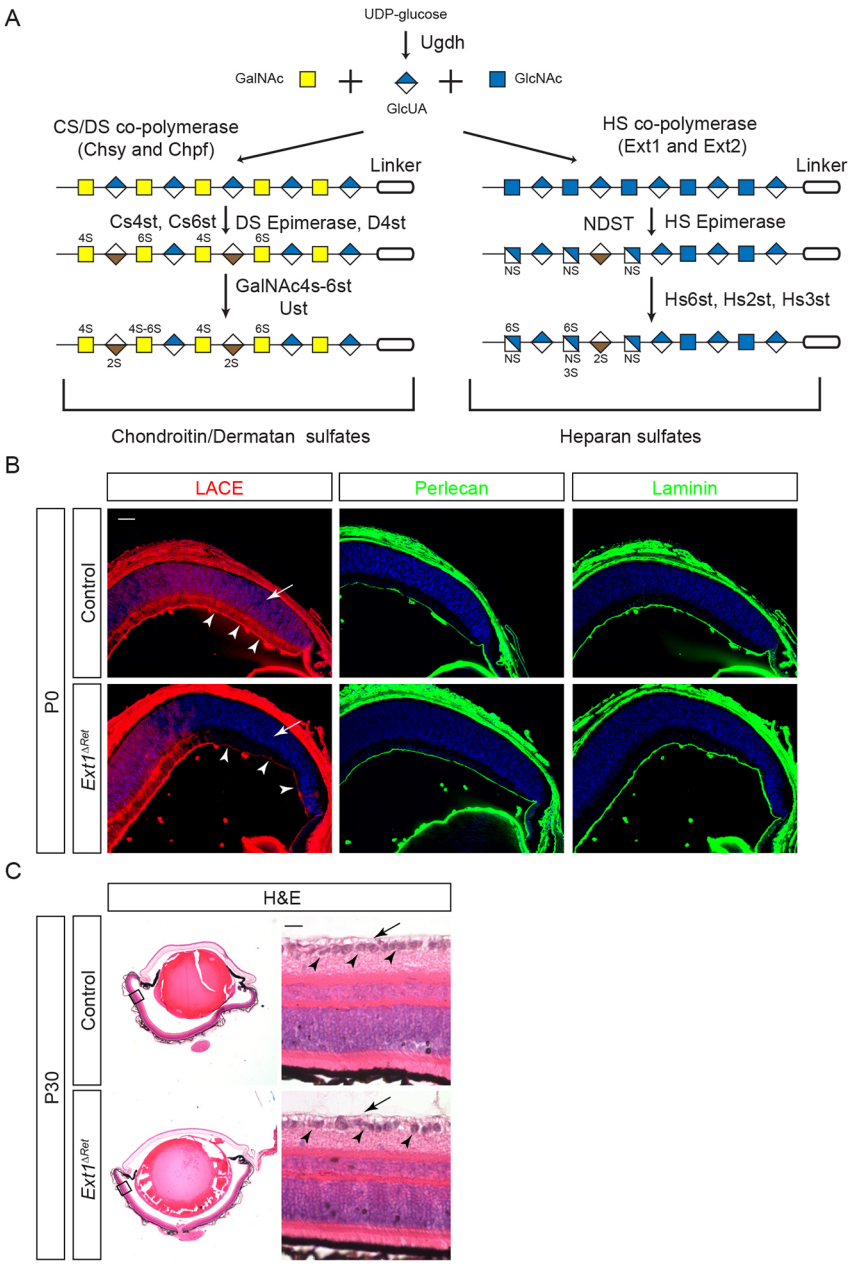

Fig. 1. Genetic deletion of *Ext1* abolishes HS biosynthesis in the retina. (A) The starting monosaccharides for GAG synthesis are glucuronic acid (GlcUA) produced by Ugdh and N-acetylgalactosamine (GalNAc) for CS/DS or N-acetylglucosamine (GlcNAc) for HS. GlcUA is concatenated with GalNAc by the CS/DS co-polymerases Chsy and Chpf, or with GlcNAc by the HS co-polymerases Ext1 and Ext2. This is followed by epimerization of GlcUA to iduronic acid (IdoUA) for DS and HS. Sulfation of CS and DS at the 4-O and 6-O positions are catalyzed first by Cs4st, Cs6st and D4st, and later by GalNAc4s-6st and Ust. In contrast, HS is first sulfated by NDST, followed by epimerization and sulfation at the 2-O, 3- and 6-O positions by Hs2st, Hs3st and Hs6st, respectively. (B) In $Ext1^{\Delta Ret}$ mutants, the LACE assay showed that HS was efficiently depleted in the peripheral neural retina (arrows), but there was still residual HS in the ILM layer (arrowheads). The ILM also maintained normal patterns of perlecan and laminin staining. (C) Histological analysis by Hematoxylin and Eosin (H&E) staining showed that retinal cells (arrowheads) remained confined within the ILM (arrows) in P30 $Ext1^{\Delta Ret}$ mutants. The panels on the right are magnified views of the boxes shown on the left. Images are representative of at least three biological replicates. Scale bars: 100 µm (B), 10 µm (C).

polymerase gene *Ext1* using *α-Cre*, which is expressed in the peripheral retina beginning at embryonic day (E) 10.5 (Cai et al., 2011; Marquardt et al., 2001). We first performed the ligand and carbohydrate engagement (LACE) assay to confirm the loss of HS. In this experiment, the presence of HS on tissue sections was detected by exogenously applied FGF10 and FGFR2B protein, which together bind avidly and specifically to sulfated HS (Pan et al., 2008). As expected, the LACE signal was observed throughout the control eye at postnatal day (P) 0, most prominently in the ILM overlying the retina (Fig. 1B, arrowheads). In contrast, *α-Cre;*$Ext1^{flox/flox}$ ($Ext1^{\Delta Ret}$) mutants displayed a specific loss of LACE signals in peripheral retinae (Fig. 1B, arrow), which corresponded to the known pattern of *α-Cre* expression. Interestingly, the LACE staining was reduced but not eliminated in the ILM above the area lacking *Ext1* expression (Fig. 1B, arrowheads), whereas the staining of perlecan, a major heparan sulfate proteoglycan (HSPG) found in the basement membrane, was unaffected. The integrity of the ILM was further confirmed by the continuous staining of laminin in $Ext1^{\Delta Ret}$ mutants. Even in P30 $Ext1^{\Delta Ret}$ mutants, we failed to observe retinal ectopias, which are usually associated with retinal cells bulging through defective ILM into the vitreous (Fig. 1C, arrows and arrowheads). These results suggest that genetic ablation of *Ext1* abrogated HS synthesis in the retina without abolishing ILM formation.

We next examined whether depletion of HS affected retinal angiogenesis, which begins with IB4-positive endothelial cells emerging from the optic disc in the neonatal mouse before spreading to the periphery of the retina (Fig. 2A). Between control and $Ext1^{\Delta Ret}$ mutants, we did not observe any statistically significant difference in the outgrowth of retinal vasculature. Nevertheless, the pruning of nascent vessels was significantly altered in $Ext1^{\Delta Ret}$ mutants, as shown by the increasing numbers of empty vessel sheaths that were positive for the basement membrane marker collagen type IV (Col IV), but negative for the endothelial marker

Development (2022) 149, dev200569. doi:10.1242/dev.200569

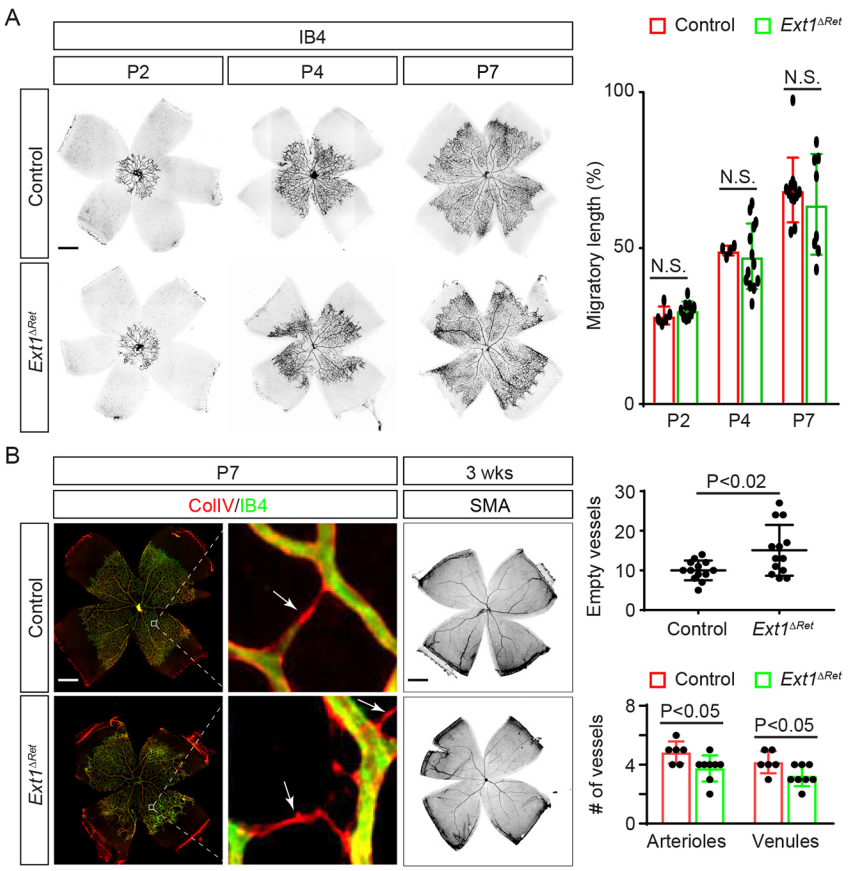

Fig. 2. Retinal HS is dispensable for initial angiogenesis but required for vascular pruning. (A) The progression of the vascular front was unaffected in *Ext1*$^{\Delta Ret}$ mutant retinae. This was quantified by measuring the migratory distance of endothelial cells in the front of the vascular plexus during postnatal development and normalized as the percentage of the radial length of the retina (unpaired two-tailed Student's *t*-test, $n>4$ retinae for each sample, N.S., not significant). (B) There was a significant increase in the number of Col IV^{+}/IB4^{-} empty vessel sheaths in *Ext1*$^{\Delta Ret}$ mutant retinae at P7 (arrows). In contrast, the number of arterioles and venules distinguishable by SMA staining was reduced. Empty vessel sheaths were counted in the middle region of the retina, whereas arterioles and venules were counted at the optic disc (unpaired two-tailed Student's *t*-test, $n=13$ retina regions for empty sheath measurement, $P<0.02$; $n>6$ retinae for vessel measurement, $P<0.05$). Scale bars: 500 µm.

IB4 (Fig. 2B, arrows). Smooth muscle actin (SMA) staining further revealed fewer arterioles and venules in 3-week-old *Ext1*$^{\Delta Ret}$ mutant retinae compared with wild-type retinae (Fig. 2B). These results showed that the retinal *Ext1* was dispensable for initial retinal angiogenesis but necessary for remodeling the vasculature.

Retinal HS is required for VEGF-dependent vessel maturation

The relatively mild vasculature defects in *Ext1*$^{\Delta Ret}$ mutant retinae raise questions as to the role of HS in VEGF signaling. In addition to inducing angiogenesis, VEGF signaling also promotes maturation of blood vessels, making them less vulnerable to a hyperoxic environment. To test this function of VEGF signaling in *Ext1*$^{\Delta Ret}$ mutants, we moved P9 pups from the room atmosphere and housed them in a 75% O_2 environment for 7 days (Fig. 3A). In control animals, this treatment led to an expected loss of capillaries in central retinae, leaving major vessels intact (Fig. 3B). In contrast, *Ext1*$^{\Delta Ret}$ mutants exhibited a far more severe vessel reduction, extending to include the peripheral retinae, and even included

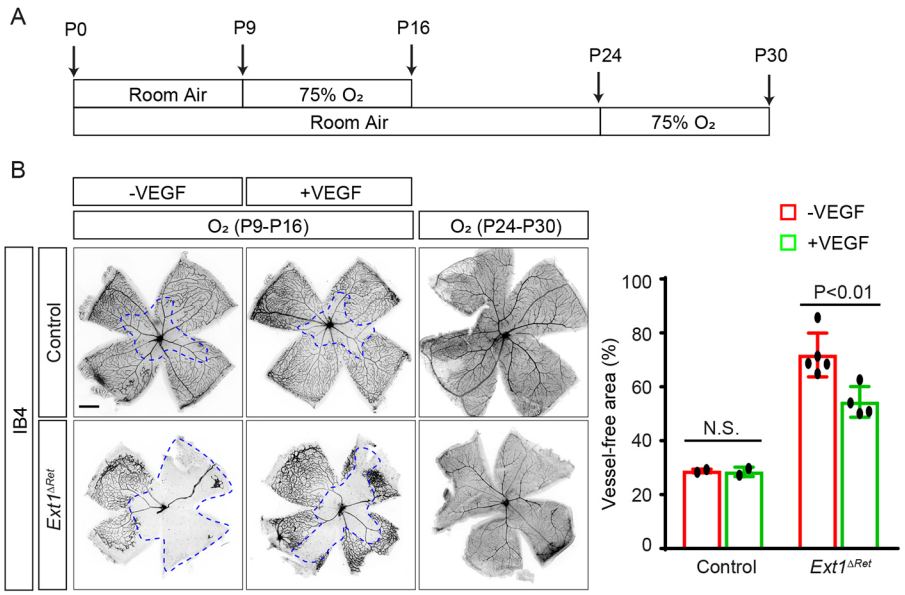

Fig. 3. VEGF ameliorates the vessel maturation defect caused by the loss of retinal HS. (A) Schematic of the hyperoxia regime. (B) Vessel ablations caused by hyperoxia treatment starting at P9 were significantly larger in *Ext1*$^{\Delta Ret}$ mutant retinae that those of controls (indicated by dashed blue lines), which were reduced by intravitreal injection of VEGFA (indicated as VEGF, 70 ng per eye). When the mice were placed in the hyperoxia environment from P24, neither the control nor the *Ext1*$^{\Delta Ret}$ mutant displayed any obvious loss of vasculature. The area of vessel ablation was measured as a percentage of the entire retina (unpaired two-tailed Student's *t*-test, $n=2$ retinae for each control group, $n>4$ retinae for *Ext1*$^{\Delta Ret}$ control mutant group. N.S., not significant, $P<0.01$). Scale bar: 500 µm (B).

Development (2022) 149, dev200569. doi:10.1242/dev.200569

arterioles and venules. However, when we postponed the hyperoxia treatment until P24, both control and *Ext1*$^{\Delta Ret}$ mutant retinae were able to maintain an intact vessel plexus, consistent with the eventual maturation of their retinal vasculatures. Therefore, the retina-specific deletion of *Ext1* delayed but did not prevent vessel maturation. We reasoned that if the delayed vessel maturation in *Ext1*$^{\Delta Ret}$ mutants was due to impaired VEGF signaling, it may be ameliorated by exogenous VEGFA. To test this hypothesis, we injected VEGFA into the vitreous of the eye at P9 prior to the hyperoxia treatment, which, unlike VEGFA injection at P7, did not substantially affect the extent of vessel ablation in wild-type animals (Alon et al., 1995). In *Ext1*$^{\Delta Ret}$ mutants, however, intravitreal injection of VEGFA led to a significant rescue of microvasculature compared with the saline-injected controls (Fig. 3B). These results support that subtle impairment of VEGF signaling leads to the vasculature defects in *Ext1*$^{\Delta Ret}$ mutants.

Deletions of genes involved in HS biosynthesis disrupt astrocyte development in the distal retina

We have previously reported severe astrocyte migration defects in *α-Cre;Ugdh*$^{flox/flox}$ mutants, in which biosynthesis of HS and CS was abolished (Tao and Zhang, 2016). This prompted us to examine whether similar defects could be observed in HS mutants. By P4, astrocytes had reached the peripheries of control retinae, but the migratory front of astrocytes appeared uneven in *Ext1*$^{\Delta Ret}$ mutants (Fig. 4A, dotted lines). As shown by Pax2 staining in control retinae, the nuclei of migrating astrocytes typically displayed spindle shapes; however, in *Ext1*$^{\Delta Ret}$ mutants, astrocyte nuclei were more rounded (Fig. 4A, insets). In contrast, the cell bodies of astrocytes labeled by Pdgfra were hyperplastic in *Ext1*$^{\Delta Ret}$ mutants, resulting in a denser astrocytic network. At the end of migration, maturing astrocytes wrap around IB4-positive blood vessels and express the glial cell marker GFAP, but heightened expression of GFAP is also a hallmark of gliosis and Müller cell activation (Yang and Wang, 2015). Compared with the uniform expression of GFAP in the control retina at P17, *Ext1*$^{\Delta Ret}$ mutants displayed significant increases in GFAP expression at the peripheries of retinae (Fig. 4A), suggesting that astrocytes in these regions were under stress.

The HS polymer generated by the Ext1 enzyme can be further modified by a number of HS sulfotransferases at N-, 2-O, 3-O or 6-O positions of the glucosamine residues (Bishop et al., 2007). To investigate the role of HS sulfation in the development and distribution of retinal astrocytes, we first genetically ablated the HS N-deacetylase and N-sulfation genes *Ndst1* and *Ndst2* in the retina. As shown by the LACE assay, sulfated HS was indeed depleted in *α-Cre;Ndst1*$^{flox/flox}$*;Ndst2*$^{-/-}$ mutants, leading to an uneven migration of astrocytes in peripheral retinae similar to that seen in *Ext1*$^{\Delta Ret}$ mutants (Fig. 4B, dotted lines). Hyaloid vessels constitute the embryonic vasculature in the vitreous that normally regresses after birth (Lang, 1997). However, *α-Cre;Ndst1*$^{flox/flox}$*;Ndst2*$^{-/-}$ mutants exhibited persistent hyaloid vessels, marked by strong LACE staining, that became attached to HS-deficient retinae (Fig. 4B, arrows). We next deleted the HS uronyl 2-O sulfotransferase gene *Hs2st* (also known as *Hs2st1*) and HS glucosaminyl 6-O sulfation genes *Hs6st1* and *Hs6st2*. Similar to *α-Cre;Ndst1*$^{flox/flox}$*;Ndst2*$^{-/-}$ mutants, we observed an uneven migration of astrocytes and persistent hyaloid vessels in the peripheral retinae of *α-Cre;Hs2st*$^{flox/flox}$*;Hs6st1*$^{flox/flox}$*;Hs6st2*$^{-/-}$ mutants. These subtle but consistent defects suggest that sulfated HS in the retina regulates astrocyte development and migration, as well as hyaloid vessel clearance.

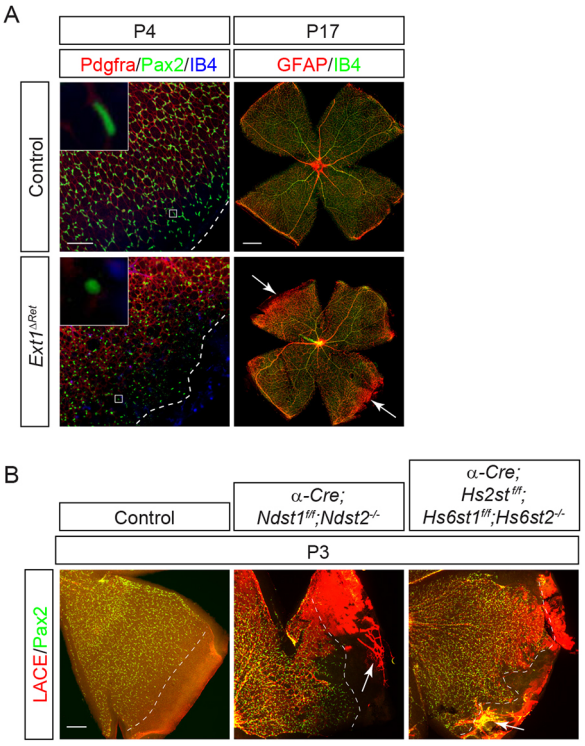

Fig. 4. Astrocyte migration is disrupted at the peripheral retina by deletion HS biosynthesis genes. (A) Migratory astrocytes in *Ext1*$^{\Delta Ret}$ mutants were uneven and sparser compared with those in controls as they approached distal retinae (dotted lines). Their nuclei shapes changed from spindle-like to round and they showed signs of stress, as indicated by hypertrophic cell bodies and elevated GFAP expression (arrows). Insets show magnified views of the boxed areas. (B) Uneven and sparser astrocytes were also observed in mutant retinae lacking genes for HS N- and O-sulfation, which also displayed abnormal penetration by hyaloid vessels (arrows). Dotted lines indicate the migratory fronts of astrocytes. Images are representative of at least three biological replicates. Scale bars: 100 µm (A, left), 500 µm (A, right), 200 µm (B).

Retinal HS potentiates astrocyte migration by promoting the assembly of the ILM

The ILM is essential for astrocyte migration and preventing abnormal penetration of hyaloid vessels into the retina (Edwards et al., 2010; Gnanaguru et al., 2013). Although the immunostaining of retinal sections did not reveal obvious defects in the ILM (Fig. 1B), we re-examined ILM integrity more thoroughly by whole-mount staining. In the majority of the P7 *Ext1*$^{\Delta Ret}$ mutant retinal regions, the ILM appeared as a smooth layer of laminin overlying the IB4-positive blood vessels (Fig. 5A). In the far periphery of mutant retinae, however, we observed scattered holes in the ILM (Fig. 5A, arrowheads). Moreover, these holes were often penetrated by residual hyaloid vessels (Fig. 5A, arrow), similar to what we observed in the peripheral retinae from mutants lacking the HS N-sulfation and O-sulfation genes. The hyaloid vessel persistence and ILM fragmentation remained in P28 *Ext1*$^{\Delta Ret}$ mutant retinae, demonstrating that the defective ILM was not repaired in adult animals.

Our data revealed that the ILM defects in *Ext1*$^{\Delta Ret}$ mutants were restricted to a narrow band at the end of the retinae, whereas a wider region of HS-depleted retinae showed an intact ILM. To reconcile the discrepancy between the restricted ILM defect and the extensive HS depletion, we considered the fact that retinal development follows a central-to-peripheral pattern. We hypothesized that because of the relatively late onset of *α-Cre* activity and persistent activity of

Development (2022) 149, dev200569. doi:10.1242/dev.200569

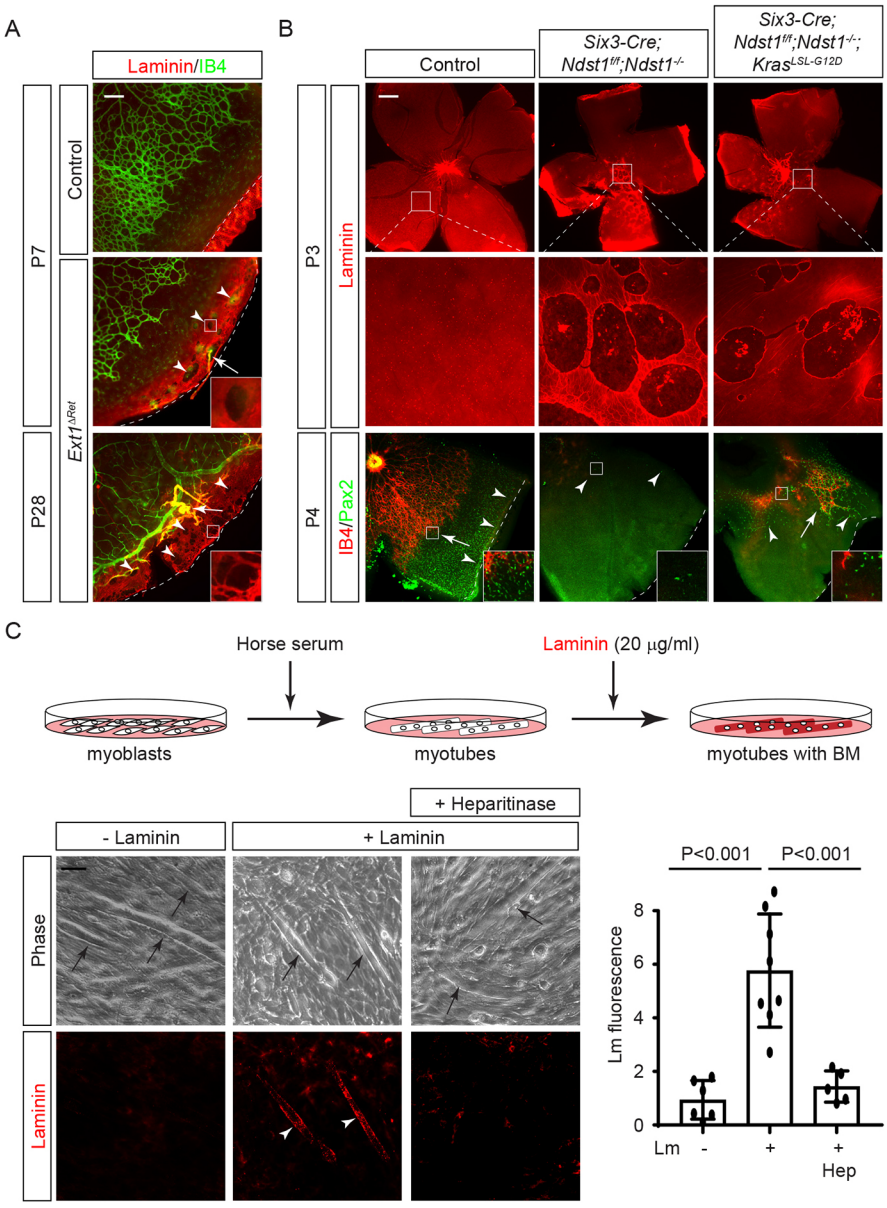

Fig. 5. Retinal HS is required for the assembly of the ILM. (A) Laminin staining revealed that the peripheral ends of P7 *Ext1*$^{\Delta Ret}$ mutant retinae contained holes in the ILM (arrowheads), which were penetrated by hyaloid vessels positive for both laminin and IB4 (arrow). These defects persisted in P28 *Ext1*$^{\Delta Ret}$ mutants (arrow and arrowheads). Dotted lines indicate edges of retinae. (B) *Six3-Cre* mediated inactivation of Ndst genes resulted in extensive ILM breaks in the central retina, which could not be rescued by constitutive Kras signaling. As a result, these mutants displayed severe defects in astrocyte migration (arrowheads) and angiogenesis (arrow). Dotted lines indicate edges of retinae. Insets show magnified views of the boxed areas in A,B. (C) After replacing FBS with horse serum, C2C12 myoblast cells fused into myotubes, which can induce exogenous laminin to polymerize on their surface. This initiation of basement membrane (BM) assembly was blocked by heparitinase (Hep) to remove the cell-surface HS. Black arrows indicate myotubes, white arrowheads indicate laminin+ myotubes. The intensities of laminin (Lm) staining in myotubes were measured using ImageJ (one-way ANOVA, n>4 myotubes for each group, P<0.001). Images are representative of at least three biological replicates. Scale bars: 100 μm (A,C), 500 μm (B).

previously expressed enzymes, much of the HS depletion may have occurred after the formation of the ILM in the mutant retinae. If this model is correct, an early Cre driver may induce much more severe disruption of the ILM. To test this hypothesis, we replaced *α-Cre* with *Six3-Cre*, which acts 1 day earlier in the central retina at E9.5 (Cai et al., 2013; Furuta et al., 2000). In *Six3-Cre;Ndst1*$^{flox/flox}$*;Ndst2*$^{-/-}$ mutants, there were indeed much larger holes in the ILM in the retina (Fig. 5B, boxes). As a result, astrocyte migration was mostly aborted, leaving only a few escaped astrocytes scattered in the retina (Fig. 5B, arrowheads). A caveat of this experiment is that HS also acts as the co-receptor for FGF signaling, which is required for development of the optic disc. However, we have previously shown that optic disc defects in both FGF receptor and *Ndst* mutants could be rescued by constitutively active Kras signaling (Cai et al., 2014). We therefore stimulated Kras signaling by inducing the oncogenic *Kras*$^{LSL-G12D}$ allele and again observed extensive ILM breaches in *Six3-Cre; Ndst1*$^{flox/flox}$*;Ndst2*$^{-/-}$*;Kras*$^{LSL-G12D}$ mutants (Fig. 5B). There were only a small number of astrocytes and associated endothelial cells in the retina, consistent with the essential roles of the ILM and HS in astrocyte migration and angiogenesis.

Thus far, study of these HS biosynthesis mutants has revealed a narrow time window for HS to affect ILM development, suggesting that HS may be required for the initial assembly of the ILM but not its later maintenance. To test this model, we turned to an *in vitro* basement membrane assembly assay (Colognato et al., 1999). In this experiment, C2C12 myoblast cells were induced to form myotubes after replacing fetal bovine serum (FBS) with horse serum in the media (Fig. 5C, arrows). Although myotubes themselves expressed little endogenous laminin, they were able to assemble *de novo* basement membrane using exogenously provided laminin (Fig. 5C, arrowheads). However, if the cell surfaces of these myotubes were first stripped of HS by heparin lyase treatment, laminin polymerization was no longer detected. This result shows that the cell-surface HS plays an important role in the assembly of the basement membrane.

CS cooperates with HS to control ILM permeability

In comparison with the HS biosynthesis mutants described above, our previously studied *α-Cre;Ugdh*$^{flox/flox}$ mutants displayed more extensive ILM defects (Tao and Zhang, 2016). One possible reason

Development (2022) 149, dev200569. doi:10.1242/dev.200569

is *Ugdh* knockout abolished biosynthesis of both HS and CS, which may have a synergistic effect on the integrity of the ILM. To investigate this possibility, we ablated the CS 4-O-sulfation enzyme C4st1 (also known as Chst11). *α-Cre;C4st1*$^{flox/flox}$ (*C4st1*$^{\Delta Ret}$) mutants did not show any obvious abnormalities in astrocyte migration and angiogenesis (Fig. 6A). As shown by laminin staining, even the combined deletion of *Ext1* and *C4st1* in *α-Cre;Ext1*$^{flox/flox}$*;C4st1*$^{flox/flox}$ (*Ext1;C4st1*$^{\Delta Ret}$) mutants failed to generate more severe ILM defects compared with those of *Ext1*$^{\Delta Ret}$ mutants (Fig. 6A, arrows).

As the deletion of C4st1 is not expected to disrupt CS function entirely, we considered the possibility that its effect on the ILM might be relatively subtle. A sensitive test for the integrity of the ILM is intravitreal injection of adeno-associated virus AAV5, which can robustly infect the retina if there are any breaches in the ILM (Dalkara et al., 2009). To detect the virally infected regions, we used a pseudotyped AAV2/5 virus that manifested the tropism of AAV5 but carried an AAV2 genome encoding the mCherry reporter. After injection into the vitreous, we detected the viral mCherry only at injection sites in both control and *C4st1*$^{\Delta Ret}$ animals (Fig. 6B, arrows), demonstrating that the barrier function of their ILMs was intact. In contrast, *Ext1*$^{\Delta Ret}$ mutants displayed mCherry expression in peripheral retinae (Fig. 6B, dotted lines), where we previously detected obvious holes in the ILM by laminin staining. Importantly, mCherry-expressing domains were significantly enlarged in *Ext1;C4st1*$^{\Delta Ret}$ mutants compared with those in *Ext1*$^{\Delta Ret}$ mutants, which matches the *α-Cre* deletion pattern in the retina. These results showed that *Ext1* and *C4st1* both contribute to the barrier function of the ILM.

Removal of GAGs disrupts the vitreoretinal interface

We next asked whether the increased permeability in *Ext1;C4st1*$^{\Delta Ret}$ mutant retinae was caused by structural abnormalities in the ILM. Transmission electron microscopy (EM) showed a continuous sheet of basement membrane beneath the control retinae at P4 (Fig. 7A, arrowheads). In contrast, there were occasional gaps in the basement membranes of the *Ext1;C4st1*$^{\Delta Ret}$ mutant (Fig. 7A, arrow), which was consistent with sporadic holes in the ILM revealed by our previous laminin staining (Fig. 6A). Interestingly, lower magnification images also revealed a layer of intermediate electron density, which separated the basement membrane from the vitreous (Fig. 7A, blue bars). In *Ext1;C4st1*$^{\Delta Ret}$ mutants, this band was not only reduced in width, but also appeared paler and less dense. Because we used an en bloc fixation and staining protocol that also highlighted glycoproteins in our EM analysis (Chuang et al., 2015; Tapia et al., 2012), this result suggested that retinal deletion of *Ext1*

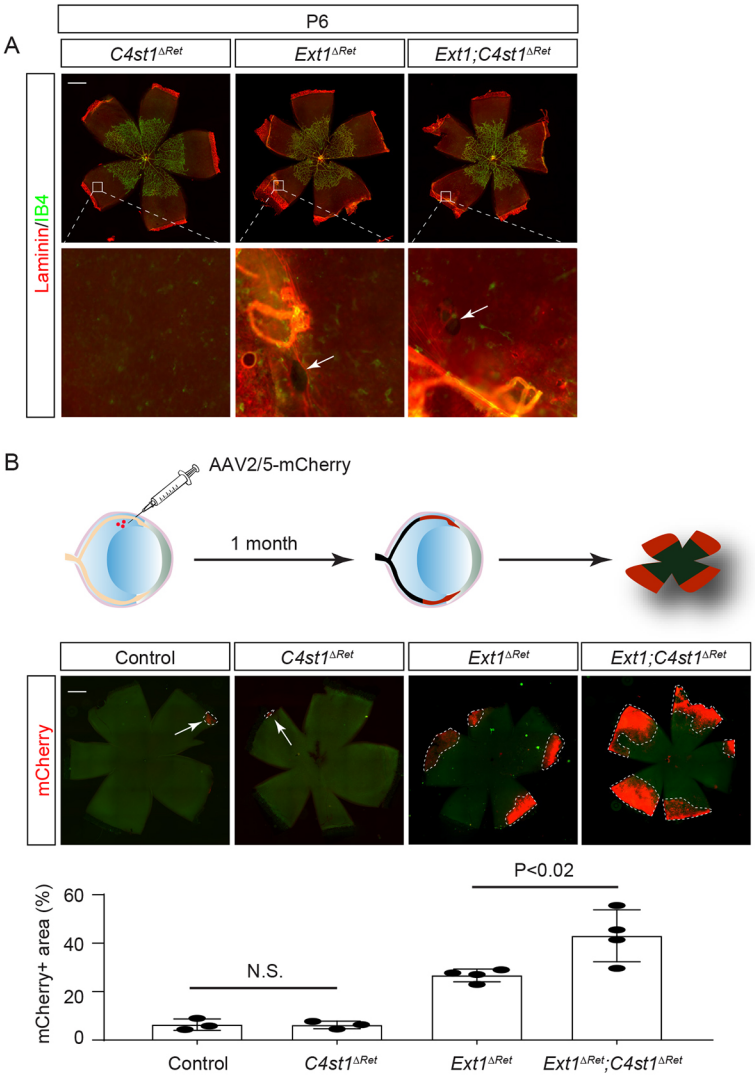

Fig. 6. The retinal CS regulates the ILM permeability with HS. (A) There were no obvious ILM holes (arrows) in *C4st1*$^{\Delta Ret}$ mutant retinae and the extent of ILM defects was comparable between the *Ext1*$^{\Delta Ret}$ and *Ext1;C4st1*$^{\Delta Ret}$ mutants. (B) One month after intravitreal injection of AAV2/5-mCherry, control and *C4st1*$^{\Delta Ret}$ mutant retinae expressed mCherry only at the injection sites (arrows), demonstrating the integrity of their ILMs. In contrast, mCherry expression was detected (areas outlined by the dotted lines) in the peripheral *Ext1*$^{\Delta Ret}$ mutant retina and significantly expanded in *Ext1;C4st1*$^{\Delta Ret}$ mutants. The areas with mCherry expression were normalized as a percentage of the entire retina (one-way ANOVA; $n>3$ retinae for each genotype; $P<0.02$; N.S., not significant). Scale bars: 500 µm.

Development (2022) 149, dev200569. doi:10.1242/dev.200569

and *C4st1* may have led to the depletion of proteoglycans in this vitreoretinal interface.

Our ultrastructure analysis showed that the thinning of the vitreoretinal interface was much more prevalent than the sporadic breaches in the basement membrane, resembling the continuous pattern of viral infection in *Ext1;C4st1*$^{\Delta Ret}$ mutant retina. This suggested that the increased permeability in the *Ext1;C4st1*$^{\Delta Ret}$ mutant may primarily be caused by disruption of this vitreoretinal interface, not just breaches in the basement membrane. We predicted that if we removed GAGs after the formation of the ILM, this increased permeability would still promote virus infection in the retina. To test this hypothesis, we injected the AAV2/5 virus with heparin lyase and chondroitin ABC lyase (ChABC), which have been shown to degrade HS and CS in the vitreous without breaking the retinal basement membrane (Balasubramani et al., 2010), into the eyes of 1-month-old animals (Fig. 7B). Consistent with our previous results, injection of the AAV2/5 virus alone induced mCherry expression only in the injection site (Fig. 7B, arrow), but when the AAV2/5 virus was co-injected with glycolytic enzymes, mCherry expression was observed in the entire retina. These data support an important role for GAGs in maintaining the retinal barrier.

DISCUSSION

In this study, we have explored the distinctive functions of HS and CS in the neural retina. By deleting the HS polymerase Ext1 in retinal progenitor cells, we demonstrate that retinal HS is dispensable for VEGF-dependent migration of endothelial cells, but it regulates the subsequent pruning and maturation of the retinal vasculature. We also show that retinal HS is required in a narrow time window for the assembly of the ILM, which is necessary for the migration of astrocytes into the retina. Lastly, we present evidence that deficient CS sulfation enhances the retinal permeability caused by HS depletion, demonstrating an important role for retina-derived CS in maintaining the barrier function. These results shed light on the multifaceted function of GAGs in growth factor signaling and ECM integrity in the retina.

It is notable that our genetic ablation of *Ext1* failed to perturb the progression of the vascular front during postnatal retinal development, yet led to a more severe oxygen-induced retinopathy (OIR) phenotype with extensive capillary loss in response to hyperoxia. At first glance, this result may appear to contradict the widely accepted model that Vegfa requires interaction with the cell-surface HS to maintain a chemo-attractive gradient for angiogenesis (Ruhrberg et al., 2002; Stalmans et al., 2002). However, it is important to consider that our conditional knockout of *Ext1* was restricted to the neural retina, leaving the lens and the optic stalk intact as potential sources of exogenous HS. Halfter and colleagues have previously performed the elegant mouse/chick transplant experiment to show that the lens synthesizes many crucial components of the ILM, including HSPGs, perlecan and collagen XVIII, whereas only agrin is expressed solely by the neural retina (Halfter et al., 2000). This explains why reduced HS staining persisted in the ILM above *Ext1* mutant retinae. In addition, the optic stalk is the source of retinal astrocytes, which migrate ahead of endothelial cells on top of the retina and express their own proteoglycans. In fact, it has previously been reported that an astrocyte-specific knockout of *Ext1* slowed down the radial expansion of the endothelial network by dampening VEGF signaling (Stenzel et al., 2011). This is in contrast to our retina-specific *Ext1* knockout, which instead disrupted the VEGF-dependent pruning and maturation of the vasculature. Therefore, the HS expressed by different ocular tissues cooperates to regulate

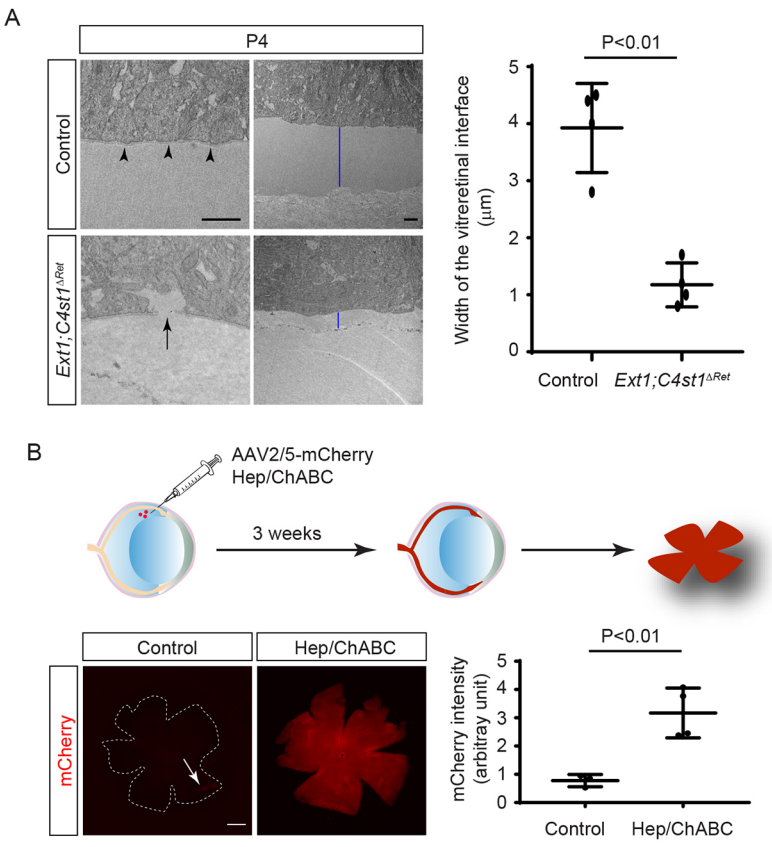

Fig. 7. The barrier function of the retinal ECM requires GAGs in the vitreoretinal interface. (A) EM analysis of *Ext1;C4st1*$^{\Delta Ret}$ mutants not only revealed occasional breaches in the retinal basement membrane (arrow), but also the shortening of a band of intermediate electron-dense materials at the vitreoretinal interface (blue bars), quantified on the right (unpaired two-tailed Student's *t*-test, $n=4$ retinal regions for each group, $P<0.01$). (B) Although mCherry expression was restricted to the site where the AAV2/5 virus was injected alone into the vitreous of 1-month-old animals (arrow), it spread to the entire retina when the virus was co-injected with glycosidic enzymes heparitinase (Hep) and chondroitinase (ChABC). The dotted line indicates the edge of the retina. Quantification of mCherry intensity is shown on the right (unpaired two-tailed Student's *t*-test, $n>3$ retinae for each control group, $P<0.01$). Scale bars: 1 μm (A), 500 μm (B).

Development (2022) 149, dev200569. doi:10.1242/dev.200569

distinctive aspects of VEGF function, orchestrating the fine-tuning of vascular development. Our findings may also have clinical significance in terms of the stability of the nascent retinal vasculature, and suggest that defects in HS expression in the retina may lead to increased vulnerability to retinopathy in premature infants (e.g. retinopathy of prematurity) without showing other obvious abnormalities in vascular development.

Another intriguing finding in our study is that α-Cre-induced abrogation of the HS polymerase gene *Ext1* disrupted ILM formation, but the breach was restricted to the far periphery of the retina. This led to abnormal migration of astrocytes in this region and penetration of hyaloid vessels into the retina, phenotypes also observed in HS N- and 6-O sulfation mutants. The limited scope of the ILM defect was not due to the lack of gene inactivation, as LACE staining on sections revealed a much larger region of HS depletion in $Ext1^{\Delta Ret}$ mutant retinae. Instead, we note that retinal development occurs in a center-to-periphery pattern. As a result, when Halfter and colleagues performed a pulse-chase experiment to study ILM regeneration *in vivo*, they found that the newly synthesized ILM was present only in the distal retina (Halfter et al., 2000). It is conceivable that, owing to the relatively late onset of the *α-Cre* driver and the persistence of residual Ext1 protein, the eventual arrest of HS biosynthesis in our $Ext1^{\Delta Ret}$ mutants coincided with the time of ILM assembly only at the far periphery of the retina. In this scenario, even if HS was lost in the more central retina already covered by the ILM, only the nascent ILM above the distal retina would be affected. This suggests that the HS derived from the neural retina is required only for the initial assembly of the ILM and not for its later maintenance. This model further predicts that the ILM could also become vulnerable to HS depletion in the central retina, provided that the onset of genetic knockout was early enough. Indeed, when we switched to an earlier retinal driver (*Six3-Cre*) to delete *Ndst* genes, we observed much larger and more numerous ILM holes in the central retina. Moreover, we showed in an *in vitro* assay that the degradation of HS prevented myotubes from promoting laminin polymerization, suggesting a general role of cell-surface HS in basement membrane assembly. This role of cell surface HS is in contrast with the roles of the secreted HS proteoglycans perlecan and collagen XVIII, which are constitutional components of the basement membrane necessary for its stability (Yurchenco and Patton, 2009). These results highlight that HS plays tissue-specific roles in the assembly and maintenance of the basement membrane.

Although we have thus far attributed the phenotype of *Ext1* knockout to the loss of HS, we also need to consider the potential gain-of-function effect of CS. It has been shown that CS biosynthesis may be upregulated in the absence of HS (Bachvarova et al., 2020). In addition, we have previously reported that deletion of the GAG biosynthesis gene *Ugdh* resulted in more severe ILM defects than *Ext1* knockout, which could be due either to differences in the enzymatic kinetics between Ugdh and Ext1 or to compensation by hyaluronan and CS. To test the latter possibility, the ideal approach would be genetic ablation of CS biosynthesis. However, unlike HS in which chain elongation can be blocked by the removal of a single enzyme (Ext1), there are four CS co-polymerase genes in the mouse genome that act redundantly, making it daunting to abrogate CS biosynthesis genetically (Bishop et al., 2007; Mikami and Kitagawa, 2013; Mizumoto et al., 2013). Thus, we opted to remove C4st1, which catalyzes the important 4-O sulfation of CS, with the understanding that biosynthesis of DS will be unaffected and that the function of CS will be at most partially impaired because C4st1 is not the only 4-O-sulfotransferase acting on CS. These reasons may explain the lack of an obvious phenotype in our *C4st1* mutants. Although the compensatory roles of hyaluronan, DS and other C4st genes await further study, using the sensitive virus infection assay, we found that loss of *C4st1* enhanced the permeability of the ILM caused by *Ext1* deficiency, revealing an important role for HS and CS in establishing the neuroretinal barrier.

How do HS and CS regulate the retinal permeability? As integral parts of the basement membrane, GAGs may play structural roles in stabilizing the ILM. However, ultrastructure analysis of our GAG mutants also revealed that a band of intermediate electron-dense materials above the basement membrane was significantly reduced. Previous studies have shown that the retinal ECM in this region is very labile (Heegaard et al., 1986; Rhodes, 1982), which may explain why it is usually missed by regular EM analysis. In contrast, we readily detected it using an EM fixation and staining protocol optimized for glycoproteins, suggesting that it is enriched in proteoglycans. This region of the retinal ECM thus resembles the glycocalyx covering endothelial cells, a gel-like coating of carbohydrates that functions as a barrier for the vasculature. Indeed, previous studies have shown that intravitreal injections of heparin and chondroitin lyases significantly increased transduction of AAV2 into the retina (Cehajic-Kapetanovic et al., 2018), although the interpretation of this result was complicated by the fact that AAV2 uses HSPG as the receptor for cellular entry. Using the pseudotyped AAV2/5 virus, we confirmed that degradation of HS and CS enhanced retinal permeability. Together, these results showed that both the basement membrane and the glycocalyx are important for maintaining the retinal barrier. Breach of the retinal barrier is the hallmark of retinopathy of prematurity, diabetic retinopathy and proliferative vitreoretinopathy. With deeper understanding of the biological function of the retinal barrier and innovative strategies to repair or stabilize its structure, the retinal basement membrane and glycocalyx may present promising therapeutic targets for preventing or curbing the harmful effects of these diseases.

MATERIALS AND METHODS

Mice

$Ndst1^{flox}$ and $Hs2st^{flox}$ mice have been previously reported (Grobe et al., 2005; Stanford et al., 2010). $Chst11^{f/f}$ mice were generated from $Chst11^{tm1a(KOMP)Wtsi}$ chimeric mice (Mutant Mouse Regional Resource Centers, MMRRC) after crossing to *Flp* mice. $Hs6st1^{flox}$ mice were a kind gift from Dr Wellington V. Cardoso (Columbia University, New York, NY, USA) (Izvolsky et al., 2008). $Ndst2^{KO}$ mice were a kind gift from Dr Lena Kjellén (University of Uppsala, Sweden) (Forsberg et al., 1999). *α-Cre* and *Six3-Cre* mice were kindly provided by Drs Ruth Ashery-Padan (Tel Aviv University, Israel) and Yasuhide Furuta (M.D. Anderson Cancer Center, Houston, TX, USA), respectively (Furuta et al., 2000; Marquardt et al., 2001). $Hs6st2^{KO}$ and $LSL\text{-}Kras^{G12D}$ mice were obtained from MMRRC and the Mouse Models of Human Cancers Consortium (MMHCC) repository at the National Cancer Institute, respectively (Tuveson et al., 2004). All mice were maintained in mixed genetic background. The floxed animals that do not carry *Cre* transgene were used as controls. All animal procedures were performed according to the protocols approved by the Columbia University's Institutional Animal Care and Use Committee and conform to the relevant regulatory standards.

Hyperoxia treatment and VEGFA injection

Neonatal mice and their nursing mother were kept in the room atmosphere from birth through P9 or P24 before being placed in a hyperoxia chamber and exposed to 75% oxygen for 7 days. Throughout this period, the P9 pups were housed with their nursing mother and the oxygen levels were

Development (2022) 149, dev200569. doi:10.1242/dev.200569

monitored electronically. Neonatal pups (P9) were anesthetized by hypothermia over ice for a few minutes. The skin over the eye was cleaned with 70% ethanol using a cotton swab and the eyelid was opened by gently cutting along the scar tissue of the prospective eyelid with a sharp 30-gauge needle. The skin was pushed away from the eye using sterile forceps, and 0.7 µl of VEGFA (100 ng/µl, #293-VE, R&D Systems) solution was injected slowly into the vitreous by inserting the glass needle at a 45° angle though the corneoscleral boundary. The eyelids were closed using cotton buds and the pups were placed on a heating mat at 37°C to recover, before they were returned to their mother.

AAV2/5 injection

Adult mice were anesthetized by intraperitoneal injection of ketamine/xylasine (071069 and 061035, Covetrus) and the breathing rate and toe-pinch reflex were monitored to ensure full anesthesia. Sterile tropicamide (070498, Covetrus) and phenylephrine hydrochloride (068882, Covetrus) drops were applied to the eye, followed by proparacaine hydrochloride eye drops (068926, Covetrus) for topical anesthesia. Lubricant eye gel was applied on each eye to prevent corneal ulcers. Using a sterile acupuncture needle, a small hole was created at the corneoscleral boundary and 0.5 µl of the AAV2/5-CMV-mCherry (1×10^{12} vg/ml, VVC-U of Iowa-4220, University of Iowa Viral Vector Core) solution was injected into the eye vitreous using a sharp microinjection glass needle. For co-injection with glycosidic enzymes, each eye also received one unit of heparin lyase (H3917, Sigma-Aldrich) and one unit of ChABC (C0773, Sigma-Aldrich) dissolved in 4 nM $CaCl_2$ and 20 mM Tris-HCl (pH 7.5). Proparacaine hydrochloride eye drops and lubricant eye gel were applied again on each eye and the mice were placed on a heating pad to recover.

Immunohistochemistry

Histology and immunohistochemistry were performed on the paraffin wax-embedded sections and cryosections as previously described (Carbe et al., 2013; Carbe and Zhang, 2011). Whole retina fixed in 4% paraformaldehyde (PFA) or 10 µm rehydrated cryosections were blocked with 10% normal goat serum for 1 h at room temperature and incubated with primary antibody overnight at 4°C. After washing with PBS, samples were incubated with the secondary fluorophore-conjugated antibody in 2% bovine serum albumin for 1 h at room temperature in the dark. Isolectin GS-IB_4 (IB4) conjugated with Alexa Fluor 488 (I21411, Thermo Fisher Scientific) was applied to visualize the vasculature. Samples were washed and mounted with n-propyl gallate anti-fading reagent (P3130, Sigma-Aldrich) and examined under a Leica DM5000-B fluorescence microscope. The following antibodies were used: anti-Col IV (1:1000, AB756P, Merck Millipore), anti-GFAP (1:1000, Z0334, Agilent Dako), anti-laminin (1:1000, L9393, Sigma-Aldrich), anti-Pax2 (1:200, PRB-276P, Covance), anti-Pdgfra (1:1000, 558774, BD Pharmingen) and anti-SMA (1:1000, M085129-2, Agilent). The anti-perlecan antibody (1:1000) was a kind gift from Dr Peter Yurchenco (Rutgers University, Piscataway, NJ, USA). The following secondary antibodies were used: Alexa Fluor 488 AffiniPure donkey anti-mouse IgG (715-545-151, 1:500) and Cy3 AffiniPure donkey anti-rabbit IgG (711-165-152, 1:1000), both from Jackson ImmunoResearch. All commercial antibodies are validated by vendors. At least three embryos of each genotype were stained for each marker.

The LACE assay was used to probe the *in situ* binding affinity of FGF-FGFR complexes to heparan sulfate on retina sections as previously described (Pan et al., 2006). Recombinant FGF10 and FGFR2B were obtained from R&D Systems.

Basement membrane assembly assay

C2C12 cells (CRL-1772, American Type Culture Collection) were authenticated and tested for contamination by the vendor and cultured in Dulbecco's Modified Eagle Medium (DMEM) with high glucose (10-013-CV, Corning) containing 10% FBS. After switching to 5% horse serum (16050130, Thermo Fisher Scientific), laminin (CB-40232, Thermo Fisher Scientific) was added at 100 µg/ml to trigger basement membrane assembly. The surface HS was removed by 1 U/ml Heparitinase I and III Blend from *Flavobacterium heparinum* (H3917, Sigma-Aldrich).

Transmission EM

For the EM experiments, eyeballs were enucleated from P4 mice under room light and were fixed in 4% PFA/0.1 M cacodylic acid overnight with their corneas partially cut open. Vibratome sections (~120 µm) were prepared from small pieces of eyecup (~2 mm×~3 mm) embedded in 5% agarose II/0.1 M cacodylic acid and post-fixed in 2.5% glutaraldehyde with 4% PFA/0.1 M cacodylic acid for 72 h. Sections were processed for en bloc fixation and staining, as previously described (Chuang et al., 2015). Briefly, after several washes in ice-cold 0.15 M cacodylate buffer containing 2 mM $CaCl_2$, the specimens were incubated with 1.5% potassium ferrocyanide, 2 mM $CaCl_2$ and 2% osmium tetroxide in 0.15 M cacodylate buffer (pH 7.4), for 1 h on ice, followed by treatment with 10 mg/ml of thiocarbohydrazide solution (01211, Polysciences) for 20 min at room temperature, and then fixation with 2% osmium tetroxide for 30 min at room temperature. The en bloc-stained tissues were dehydrated with graded ethanol and embedded in Epon. Ultrathin sections (72 nm) were collected on G400-Cu grids (Electron Microscopy Sciences) and were examined under a Hitachi HT7800 electron microscope for conventional transmission EM analysis.

Quantification and statistical analysis

The migratory lengths of blood vessels and the areas of retinae were measured using ImageJ. For quantification of staining, fluorescent images were converted to grayscale and mean intensities were measured using ImageJ. Statistical analysis was performed using GraphPad Prism 7. Sample sizes were not predetermined. Data represent mean±s.d. Unpaired two-tailed Student's *t*-test was used for comparing two conditions and one-way ANOVA with Tukey's multi-comparison test for three or more conditions.

Acknowledgements

The authors thank Peter Yurchenco for the perlecan antibody and Drs Wellington V. Cardoso, Yasuhide Furuta, Lena Kjellén, Ruth Ashery-Padan for mice. We thank one of the anonymous reviewers for suggesting EM analysis. We also thank members of Zhang lab for discussion.

Competing interests

The authors declare no competing or financial interests.

Author contributions

Conceptualization: C.T., X.Z.; Methodology: C.T.; Formal analysis: C.T., J.-Z.C.; Investigation: C.T., N.M., J.-Z.C., Y.W.; Data curation: C.T.; Writing - original draft: C.T., X.Z.; Writing - review & editing: C.T., S.E.B., J.D.E., C.-H.S., X.Z.; Supervision: C.T., C.-H.S., X.Z.; Project administration: C.T., X.Z.; Funding acquisition: C.T., C.-H.S., J.D.E., X.Z.

Funding

The work was supported by grants from the National Institutes of Health (NIH; EY017061, EY018868, EY025933 and EY031210 to X.Z.; HL107150 and HL57345 to J.D.E.; EY029428 and EY032966 to C.-H.S.). The Columbia Ophthalmology Core Facility are supported by the NIH Core grant 5P30EY019007 and unrestricted funds from Research to Prevent Blindness (RPB). C.T. is a recipient of the Jonas Scholar award granted by The Barbara and Donal Jonas Family Fund. X.Z. is supported by a Jules and Doris Stein Research to Prevent Blindness Professorship. Deposited in PMC for release after 12 months.

Peer review history

The peer review history is available online at https://journals.biologists.com/dev/article-lookup/doi/10.1242/dev.200569.

References

Alon, T., Hemo, I., Itin, A., Pe'er, J., Stone, J. and Keshet, E. (1995). Vascular endothelial growth factor acts as a survival factor for newly formed retinal vessels and has implications for retinopathy of prematurity. *Nat. Med.* **1**, 1024-1028. doi:10.1038/nm1095-1024

Bachvarova, V., Dierker, T., Esko, J., Hoffmann, D., Kjellen, L. and Vortkamp, A. (2020). Chondrocytes respond to an altered heparan sulfate composition with distinct changes of heparan sulfate structure and increased levels of chondroitin sulfate. *Matrix Biol.* **93**, 43-59. doi:10.1016/j.matbio.2020.03.006

Balasubramani, M., Schreiber, E. M., Candiello, J., Balasubramani, G. K., Kurtz, J. and Halfter, W. (2010). Molecular interactions in the retinal basement membrane system: a proteomic approach. *Matrix Biol.* **29**, 471-483. doi:10.1016/j.matbio.2010.04.002

Bishop, J. R., Schuksz, M. and Esko, J. D. (2007). Heparan sulphate proteoglycans fine-tune mammalian physiology. *Nature* **446**, 1030-1037. doi:10.1038/nature05817

Cai, Z., Grobe, K. and Zhang, X. (2014). Role of heparan sulfate proteoglycans in optic disc and stalk morphogenesis. *Dev. Dyn.* **243**, 1310-1316. doi:10.1002/dvdy.24142

Cai, Z., Simons, D. L., Fu, X. Y., Feng, G. S., Wu, S. M. and Zhang, X. (2011). Loss of Shp2-mediated mitogen-activated protein kinase signaling in muller glial cells results in retinal degeneration. *Mol. Cell. Biol.* **31**, 2973-2983. doi:10.1128/MCB.05054-11

Cai, Z., Tao, C., Li, H., Ladher, R., Gotoh, N., Feng, G. S., Wang, F. and Zhang, X. (2013). Deficient FGF signaling causes optic nerve dysgenesis and ocular coloboma. *Development* **140**, 2711-2723. doi:10.1242/dev.089987

Carbe, C. and Zhang, X. (2011). Lens induction requires attenuation of ERK signaling by Nf1. *Hum. Mol. Genet.* **20**, 1315-1323. doi:10.1093/hmg/ddr014

Carbe, C., Garg, A., Cai, Z., Li, H., Powers, A. and Zhang, X. (2013). An allelic series at the paired box gene 6 (Pax6) locus reveals the functional specificity of Pax genes. *J. Biol. Chem.* **288**, 12130-12141. doi:10.1074/jbc.M112.436865

Cehajic-Kapetanovic, J., Milosavljevic, N., Bedford, R. A., Lucas, R. J. and Bishop, P. N. (2018). Efficacy and Safety of Glycosidic Enzymes for Improved Gene Delivery to the Retina following Intravitreal Injection in Mice. *Mol. Ther. Method. Clin. Dev.* **9**, 192-202. doi:10.1016/j.omtm.2017.12.002

Chuang, J. Z., Hsu, Y. C. and Sung, C. H. (2015). Ultrastructural visualization of trans-ciliary rhodopsin cargoes in mammalian rods. *Cilia* **4**, 4. doi:10.1186/s13630-015-0013-1

Colognato, H., Winkelmann, D. A. and Yurchenco, P. D. (1999). Laminin polymerization induces a receptor-cytoskeleton network. *J. Cell Biol.* **145**, 619-631. doi:10.1083/jcb.145.3.619

Dalkara, D., Kolstad, K. D., Caporale, N., Visel, M., Klimczak, R. R., Schaffer, D. V. and Flannery, J. G. (2009). Inner limiting membrane barriers to AAV-mediated retinal transduction from the vitreous. *Mol. Ther.* **17**, 2096-2102. doi:10.1038/mt.2009.181

Edwards, M. M., Mammadova-Bach, E., Alpy, F., Klein, A., Hicks, W. L., Roux, M., Simon-Assmann, P., Smith, R. S., Orend, G., Wu, J. et al. (2010). Mutations in Lama1 disrupt retinal vascular development and inner limiting membrane formation. *J. Biol. Chem.* **285**, 7697-7711. doi:10.1074/jbc.M109.069575

Forsberg, E., Pejler, G., Ringvall, M., Lunderius, C., Tomasini-Johansson, B., Kusche-Gullberg, M., Eriksson, I., Ledin, J., Hellman, L. and Kjellen, L. (1999). Abnormal mast cells in mice deficient in a heparin-synthesizing enzyme. *Nature* **400**, 773-776. doi:10.1038/23488

Furuta, Y., Lagutin, O., Hogan, B. L. and Oliver, G. C. (2000). Retina- and ventral forebrain-specific Cre recombinase activity in transgenic mice. *Genesis* **26**, 130-132. doi:10.1002/(SICI)1526-968X(200002)26:2<130::AID-GENE9>3.0.CO;2-I

Gnanaguru, G., Bachay, G., Biswas, S., Pinzon-Duarte, G., Hunter, D. D. and Brunken, W. J. (2013). Laminins containing the beta 2 and gamma 3 chains regulate astrocyte migration and angiogenesis in the retina. *Development* **140**, 2050-2060. doi:10.1242/dev.087817

Grobe, K., Inatani, M., Pallerla, S. R., Castagnola, J., Yamaguchi, Y. and Esko, J. D. (2005). Cerebral hypoplasia and craniofacial defects in mice lacking heparan sulfate Ndst1 gene function. *Development* **132**, 3777-3786. doi:10.1242/dev.01935

Halfter, W., Dong, S., Schurer, B., Osanger, A., Schneider, W., Ruegg, M. and Cole, G. J. (2000). Composition, synthesis, and assembly of the embryonic chick retinal basal lamina. *Dev. Biol.* **220**, 111-128. doi:10.1006/dbio.2000.9649

Heegaard, S., Jensen, O. A. and Prause, J. U. (1986). Structure and composition of the inner limiting membrane of the retina. SEM on frozen resin-cracked and enzyme-digested retinas of Macaca mulatta. *Graefes Arch. Clin. Exp. Ophthalmol.* **224**, 355-360. doi:10.1007/BF02150029

Izvolsky, K. I., Lu, J., Martin, G., Albrecht, K. H. and Cardoso, W. V. (2008). Systemic inactivation of Hs6st1 in mice is associated with late postnatal mortality without major defects in organogenesis. *Genesis* **46**, 8-18. doi:10.1002/dvg.20355

Lang, R. A. (1997). Apoptosis in mammalian eye development: lens morphogenesis, vascular regression and immune privilege. *Cell Death Differ.* **4**, 12-20. doi:10.1038/sj.cdd.4400211

Marquardt, T., Ashery-Padan, R., Andrejewski, N., Scardigli, R., Guillemot, F. and Gruss, P. (2001). Pax6 is required for the multipotent state of retinal progenitor cells. *Cell* **105**, 43-55. doi:10.1016/S0092-8674(01)00295-1

Mikami, T. and Kitagawa, H. (2013). Biosynthesis and function of chondroitin sulfate. *Biochim. Biophys. Acta* **1830**, 4719-4733. doi:10.1016/j.bbagen.2013.06.006

Mizumoto, S., Ikegawa, S. and Sugahara, K. (2013). Human genetic disorders caused by mutations in genes encoding biosynthetic enzymes for sulfated glycosaminoglycans. *J. Biol. Chem.* **288**, 10953-10961. doi:10.1074/jbc.R112.437038

Pan, Y., Carbe, C., Powers, A., Zhang, E. E., Esko, J. D., Grobe, K., Feng, G. S. and Zhang, X. (2008). Bud specific N-sulfation of heparan sulfate regulates Shp2-dependent FGF signaling during lacrimal gland induction. *Development* **135**, 301-310. doi:10.1242/dev.014829

Pan, Y., Woodbury, A., Esko, J. D., Grobe, K. and Zhang, X. (2006). Heparan sulfate biosynthetic gene Ndst1 is required for FGF signaling in early lens development. *Development* **133**, 4933-4944. doi:10.1242/dev.02679

Rhodes, R. H. (1982). An ultrastructural study of the complex carbohydrates of the mouse posterior vitreoretinal juncture. *Invest. Ophthalmol. Vis. Sci.* **22**, 460-477.

Ruhrberg, C., Gerhardt, H., Golding, M., Watson, R., Ioannidou, S., Fujisawa, H., Betsholtz, C. and Shima, D. T. (2002). Spatially restricted patterning cues provided by heparin-binding VEGF-A control blood vessel branching morphogenesis. *Genes Dev.* **16**, 2684-2698. doi:10.1101/gad.242002

Stalmans, I., Ng, Y. S., Rohan, R., Fruttiger, M., Bouche, A., Yuce, A., Fujisawa, H., Hermans, B., Shani, M., Jansen, S. et al. (2002). Arteriolar and venular patterning in retinas of mice selectively expressing VEGF isoforms. *J. Clin. Invest.* **109**, 327-336. doi:10.1172/JCI0214362

Stanford, K. I., Wang, L., Castagnola, J., Song, D., Bishop, J. R., Brown, J. R., Lawrence, R., Bai, X., Habuchi, H., Tanaka, M. et al. (2010). Heparan sulfate 2-O-sulfotransferase is required for triglyceride-rich lipoprotein clearance. *J. Biol. Chem.* **285**, 286-294. doi:10.1074/jbc.M109.063701

Stenzel, D., Lundkvist, A., Sauvaget, D., Busse, M., Graupera, M., van der Flier, A., Wijelath, E. S., Murray, J., Sobel, M., Costell, M. et al. (2011). Integrin-dependent and -independent functions of astrocytic fibronectin in retinal angiogenesis. *Development* **138**, 4451-4463. doi:10.1242/dev.071381

Tao, C. and Zhang, X. (2014). Development of astrocytes in the vertebrate eye. *Dev. Dyn.* **243**, 1501-1510. doi:10.1002/dvdy.24190

Tao, C. and Zhang, X. (2016). Retinal proteoglycans act as cellular receptors for basement membrane assembly to control astrocyte migration and angiogenesis. *Cell Rep.* **17**, 1832-1844. doi:10.1016/j.celrep.2016.10.035

Tapia, J. C., Kasthuri, N., Hayworth, K. J., Schalek, R., Lichtman, J. W., Smith, S. J. and Buchanan, J. (2012). High-contrast en bloc staining of neuronal tissue for field emission scanning electron microscopy. *Nat. Protoc.* **7**, 193-206. doi:10.1038/nprot.2011.439

Tuveson, D. A., Shaw, A. T., Willis, N. A., Silver, D. P., Jackson, E. L., Chang, S., Mercer, K. L., Grochow, R., Hock, H., Crowley, D. et al. (2004). Endogenous oncogenic K-ras(G12D) stimulates proliferation and widespread neoplastic and developmental defects. *Cancer Cell* **5**, 375-387. doi:10.1016/s1535-6108(04)00085-6

Yang, Z. and Wang, K. K. (2015). Glial fibrillary acidic protein: from intermediate filament assembly and gliosis to neurobiomarker. *Trends Neurosci.* **38**, 364-374. doi:10.1016/j.tins.2015.04.003

Yurchenco, P. D. and Patton, B. L. (2009). Developmental and pathogenic mechanisms of basement membrane assembly. *Curr. Pharm. Des.* **15**, 1277-1294. doi:10.2174/138161209787846766